

Reliability Enhancement for VR Delivery in Mobile-Edge Empowered Dual-Connectivity μ Wave-mmWave HetNets

Zhuojia Gu, Hancheng Lu, Peilin Hong, and Yongdong Zhang

Abstract

The reliability of current virtual reality (VR) delivery is low due to the limited resources on VR head-mounted displays (HMDs) and the transmission rate bottleneck of sub-6 GHz (μ Wave) networks. In this paper, we propose a dual-connectivity μ Wave-mmWave heterogeneous network architecture empowered by mobile edge capability. The core idea of the proposed architecture is to utilize the complementary advantages of μ Wave links and mmWave links to conduct a collaborative edge resource design, which aims to improve the reliability of VR delivery. From the perspective of stochastic geometry, we analyze the reliability of VR delivery and theoretically demonstrate that μ Wave links can be used to enhance the reliability of VR delivery despite the large mmWave bandwidth. Based on our analytical work, we formulate a joint caching and computing optimization problem with the goal to maximize the reliability of VR delivery. By analyzing the coupling caching and computing strategies at HMDs, μ Wave and mmWave base stations (BSs), we further transform the problem into a multiple-choice multi-dimension knapsack problem. A best-first branch and bound algorithm and a difference of convex programming algorithm are proposed to obtain the optimal and sub-optimal solution, respectively. Numerical results demonstrate the performance improvement using the proposed algorithms, and reveal that caching more monocular videos at μ Wave BSs and more stereoscopic videos at mmWave BSs can improve the VR delivery reliability efficiently.

Index Terms

Virtual reality, μ Wave-mmWave heterogeneous networks, reliability enhancement, mobile edge computing, stochastic geometry.

I. INTRODUCTION

In recent years, the interest of virtual reality (VR) in academia and industry has been unprecedented [1]. To achieve the immersive experience, the most important task is to increase the resolution of VR applications to the resolution of human eyes [2]. It is impractical to cache all rendered VR videos locally at VR head-mounted displays (HMDs) in advance, especially in the scenarios where user interactions are required. Moreover, users prefer to experience VR videos anytime and anywhere, compared with being tied down by wired cables. Therefore, VR videos are expected to be delivered real-time over wireless networks. However, the bandwidth required for delivering VR videos is usually 4-5 times the bandwidth required for delivering conventional high-definition videos [3], which puts tremendous pressure on the network bandwidth. On the other hand, VR applications are typical ultra-reliable low-latency communication (URLLC) applications, and the end-to-end delay exceeding 20 ms can cause dizziness of users [4]. Thus, it is essential to ensure the high reliability of VR delivery networks, which means that ensuring more data packets delivered to HMDs within the latency requirement of VR applications for a satisfactory VR viewing experience. In this regard, two fundamental problems for VR delivery should be addressed: *1) How to enhance the reliability of VR delivery when delivering a large amount of video data over wireless networks, and 2) how to enhance the reliability of VR delivery when performing time-consuming projecting and rendering of raw VR viewpoints?*

For the first problem, using the current sub-6 GHz (μ Wave) network is limited by the bottleneck of wireless bandwidth and cannot meet the URLLC requirements of VR applications. The sufficient spectrum resources brought by millimeter wave (mmWave) communication are considered to be the key enablers of 5G applications. Sufficient bandwidth resources make it possible to transmit large-capacity VR videos in real time. However, mmWave signals are prone to be blocked and suffer severe fading. This poses a great challenge to VR applications, because users may frequently experience blockage caused by buildings, human bodies, and environmental facilities. To tackle the problem, dual-connectivity (DC) μ Wave-mmWave heterogeneous networks (HetNets) are promising for enhancing the reliability of VR delivery. DC is an appealing technique for performance enhancement in wireless networks, and it allows the user to have two simultaneous connections and utilize both radio resources [5]. Inherently, DC μ Wave-mmWave HetNets utilize the complementary advantages of the wide signal coverage in μ Wave networks and sufficient spectrum resources in mmWave networks, which is suitable

for reliability enhancement of VR delivery.

For the second problem, computation offloading is seen as a key enabler to provide the required video projection rendering capabilities for VR delivery. Edge computing servers are suitable for performing high CPU- and GPU-intensive computing tasks. By providing efficient computing resources close to users, mobile edge computing (MEC) strikes a balance between communication delay and computing delay. Specifically, the HMD can upload the tracking information (e.g., game actions or viewpoint preferences) to the MEC server to offload computing tasks, and the MEC server sends the downlink SVs to the HMD. In addition, the caching capability of MEC servers can help save the projection and rendering time.

Based on the above discussion, in this paper, we propose a mobile-edge empowered dual-connectivity (DC) μ Wave-mmWave HetNet architecture, and aim to conduct a collaborative design of edge network resources to enhance the reliability of VR delivery.

A. Related Work

1) *Reliability Enhancement for Wireless Transmission*: Ultra-reliable communication has become the vital support of mission-critical 5G applications. Mei *et al.* [6] proposed a reliability guaranteed resource allocation scheme in vehicle-to-vehicle (V2V) networks. Guo *et al.* [7] extended the research to perform a reliability-aware resource allocation in V2V networks based only on large-scale fading channel information. Popovski *et al.* [8] analyzed the fundamental tradeoffs between ultra-reliability and some other metrics (i.e., latency, bandwidth occupancy and energy consumption) for wireless access. Recently, the joint application of μ Wave and mmWave in HetNets has been proposed as an attractive solution to improve the network performance [9]. Semiari *et al.* [10], [11] introduced DC mode into μ Wave-mmWave HetNets to ensure data transmission reliability while considering the user association and scheduling. DC implements carrier aggregation between sites through base station coordination to realize diversified association, which can reduce the handover failure and wireless link failure, thus improving the transmission reliability. DC mode has been extended to multi-connectivity (MC) mode in [12], [13], which enables simultaneous connections of multiple air interfaces such as cellular, device-to-device (D2D) and WiFi links to further support ultra-reliable applications.

2) *Mobile Edge Computing for VR delivery*: Authors in [2], [14], [15] inspired the use of MEC resources for VR delivery to obtain the potential performance gain, but they did not establish theoretical formulation and provided efficient algorithms. Some efficient task offloading

algorithms in wireless cellular networks with MEC were proposed in [16]–[20]. The MEC task offloading technology was introduced for the delivery of VR video in [21]–[23]. Sun *et al.* [21] focused on balancing the local and edge computing resources to maximize the average bandwidth usage for VR delivery. Dang *et al.* [22] extended the scenario in [21] to an edge fog computing network to achieve an economical computing offloading scheme that minimized the average delay for VR delivery. Chakareski *et al.* [23] proposed an edge server cooperation framework to efficiently offload the local computing tasks. It is worth noting that [21]–[23] focused on improving the average bandwidth usage or delivery latency in MEC empowered VR delivery networks. Nevertheless, little work has focused on improving the reliability of VR delivery.

B. Contributions

As presented in existing related works, wireless channels and connections have a significant impact on the reliability of data transmission. In the context of VR delivery, these wireless factors have not been well studied. First, channel conditions highly depend on the random locations of base stations and wireless channel fadings, and the reliability of VR delivery depends to a large extent on the probability of the link outage caused by the impairment of signal-to-interference-ratio (SINR). However, the impact of wireless channel fluctuation on the reliability of VR delivery is largely overlooked in the existing literatures. Second, although the dual-connectivity μ Wave-mmWave technology has been proved to improve the reliability of data transmission, existing works on VR delivery mostly assumed single-connectivity (i.e., one wireless interface) for a HMD (e.g., see [16]–[23]). These works mainly focused on the task offloading of VR video projection and rendering in the MEC scenario. Nevertheless, DC is considered as a promising technology for realizing URLLC applications, while the resource coordination for VR delivery in DC μ Wave-mmWave HetNets with MEC is challenging when the interface diversity is implemented. On the one hand, it is essential to decide whether to deliver the viewpoint over μ Wave links or mmWave links when the requested viewpoint is not cached locally. This should not only consider the influence of the wireless channel conditions, but also consider whether the requested viewpoint is cached at μ Wave BSs (μ BSs) or mmWave BSs (mBSs), as well as the impact of the limited computation resources of HMDs, μ BSs and mBSs on the computation delay. On the other hand, a proper resource coordination between μ Wave networks and mmWave networks is vital for adapting the computation-intensive VR videos. Specifically, local cache can save the transmission delay of viewpoints at the cost of

occupying limited local caching capacity. Caching simultaneously at μ BSs and mBSs can reduce the transmission delay of some popular viewpoints with a higher probability, but at the cost of occupying more caching capacity of BSs compared with caching at either μ BSs or mBSs. In addition, the caching and computing strategies in DC μ Wave-mmWave HetNets are coupled. If monocular videos (MVs) are cached at μ BSs or mBSs, the caching capacity can be saved, but the computation time for projection and rendering is increased. While caching stereoscopic videos (SVs) save the computation time at the cost of more caching capacity.

To address the aforementioned issues, in this paper, we utilize tools from stochastic geometry to model the DC μ Wave-mmWave channels and theoretically analyze the reliability of VR delivery by comprehensively considering the influence of communication, caching, and computation. We then perform the resource coordination and jointly optimize the caching and computing strategy, aiming to ensure higher reliability of VR delivery. The main contributions of this paper are summarized as follows:

- We propose a DC μ Wave-mmWave HetNet architecture empowered by mobile edge caching and computing capability, aiming to meet the requirement of ultra reliability of VR delivery. In the proposed architecture, we conduct a collaborative design of resource utilization by considering the complementary advantages of μ Wave and mmWave links, and the impact of caching and computation on the reliability of VR delivery.
- Based on stochastic geometry framework, we derive closed-form expressions for the reliability of VR delivery in the DC μ Wave-mmWave HetNet. We propose a link selection strategy based on the minimum-delay delivery, and derive the VR delivery probability over μ Wave links and mmWave links. The relationship between the delivery probability and the difference of caching and computing strategy in μ Wave and mmWave tiers is provided. We theoretically demonstrate that μ Wave links can be used to enhance the reliability of VR delivery despite the large mmWave bandwidth.
- We formulate the joint caching and computing optimization problem based on our analytical work. By analyzing the coupling relationship between caching and computing strategies at HMDs, μ BSs and mBSs, we transform the problem into a multiple-choice multi-dimension knapsack problem (MMKP). We propose a best-first branch and bound algorithm (BFBB) by calculating the upper and lower bounds of the MMKP to obtain the optimal solution. To further reduce the complex of the algorithm, the problem is transformed into a continuous optimization problem, and the difference of convex programming technique is utilized to

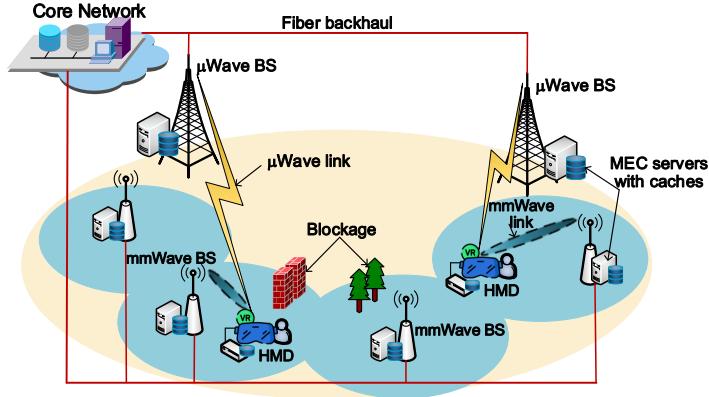


Fig. 1. Dual-connectivity μ Wave-mmWave heterogeneous network architecture empowered by mobile edge capability.

obtain a sub-optimal solution.

- We conduct numerical evaluation to validate the theoretical analysis of reliability with respect to several key parameters, such as blockage density, CPU cycles, and cache size of μ BSs/mBSs/HMDs. Numerical results show great promise of the proposed DC μ Wave-mmWave HetNet architecture to enhance the reliability of VR delivery. The results also reveal that it is more advantageous to cache MVs at μ BSs and cache SVs at mBSs for enhancing the reliability efficiently.

The rest of this paper is organized as follows. We first introduce the system model in Section II. We then analyze the reliability of VR delivery over DC μ Wave-mmWave HetNets and provide the link selection strategy to formulate the joint caching and computing problem in Section III. In Section IV, we first provide the BFBB algorithm based on the computation of upper and lower bounds of the optimal solution, and a difference of convex programming algorithm with lower complexity is proposed to maximize the reliability of VR delivery. Numerical results are provided in Section V and Section VI concludes this paper with summary.

II. SYSTEM MODEL

A. Network Model

As illustrated in Fig. 1, we consider the VR delivery in a two-tier dual-connectivity (DC) μ Wave-mmWave HetNet. The locations of μ BSs and mBSs are modeled as two independent and homogeneous Poisson Point Processes (PPPs), which are denoted by Φ_μ , Φ_m of densities λ_μ , λ_m , respectively. DC is implemented at HMDs by performing packet data convergence protocol (PDCP) layer integration [24], so a HMD can be simultaneously connected to a μ BS and a

mBSs. Instead of delivering 360° VR videos, μ BSs and mBSs only deliver the requested MVs and SVs. As mentioned above, MVs are projected and rendered using the computing resources at BSs or HMDs to create SVs. The set of all viewpoints is denoted by $\mathcal{J} = \{1, 2, \dots, J\}$. Each viewpoint $j \in \mathcal{J}$ corresponds to an MV and an SV. The data sizes of the j -th MV and SV are denoted by d_j^M and d_j^S , respectively. Note that d_j^S is at least twice larger than d_j^M , i.e., $d_j^S/d_j^M \geq 2$, due to the creation of stereoscopic video.

In the μ Wave tier, all channels undergo independent identically distributed (i.i.d.) Rayleigh fading. Without loss of generality, when a HMD located at the origin o requests the j -th viewpoint from the associated μ BS, its received signal-to-interference-plus-noise ratio (SINR) is given by,

$$\Upsilon_j^\mu = \frac{P_\mu h_j^\mu r^{-\alpha_\mu}}{I_j^\mu + \sigma_\mu^2}, \quad (1)$$

where P_μ is the transmit power of μ BS, h_j^μ is the Rayleigh channel gain between the HMD and its serving μ BS which follows the exponential distribution. $r^{-\alpha_\mu}$ is the path loss with the distance r , where α_μ is the path loss exponent. $I_j^\mu = \sum_{n \in \Phi_\mu \setminus b_\mu} P_\mu h_j^{\mu,n} r^{-\alpha_\mu,n}$ denotes the inter-cell interference, where b_μ denotes the associated μ BS. σ_μ^2 is the noise power of a μ Wave link.

In the mmWave tier, unlike the conventional μ Wave counterpart, mmWave transmissions are highly sensitive to blockage. We adopt a two-state statistical blockage model for each mmWave link as in [25], such that the probability of the link to be LOS or NLOS is a function of the distance between the HMD and its serving mBS. Assume that the distance between them is r , then the probability that a link of length r is LOS or NLOS can be modeled as

$$\rho_L(r) = e^{-\kappa r}, \quad \rho_N(r) = 1 - e^{-\kappa r}, \quad (2)$$

respectively, where κ is the decay rate depending on the blockage parameter and density [26]. Assume that the antenna arrays at mBSs and HMDs perform directional beamforming with the main lobe directed towards the dominant propagation path and having less radiant energy in other directions. For tractability in the analysis, we adopt a sectorial antenna pattern [27]. Denote θ as the main lobe beamwidth, and M and m as the directivity gain of main and side lobes, respectively. Then the random antenna gain/interference G between the mBS and the HMD has 3 patterns with different probabilities, which is given as

$$G = \begin{cases} M^2, & \text{with prob. } \left(\frac{\theta}{2\pi}\right)^2, \\ Mm, & \text{with prob. } \frac{2\theta(2\pi - \theta)}{(2\pi)^2}, \\ m^2, & \text{with prob. } \left(\frac{2\pi - \theta}{2\pi}\right)^2. \end{cases} \quad (3)$$

Independent Nakagami fading is assumed for each link. Parameters of Nakagami fading N_L and N_N are assumed for LOS and NLOS links, respectively. Therefore, when the HMD requests the j -th viewpoint from its associated mBS, the received SINR is given by

$$\Upsilon_j^m = \frac{P_m h_j^m G r^{-\alpha_m}}{I_j^m + \sigma_m^2}, \quad (4)$$

where P_m is the transmit power of the mBS, h_j^m is the Nakagami channel fading which follows Gamma distribution. The path loss exponent $\alpha_m = \alpha_L$ when it is a LOS link and $\alpha_m = \alpha_N$ when it is an NLOS link. $I_j^m = \sum_{n \in \Phi_m \setminus b_m} P_m h_j^{m,n} r^{-\alpha_{m,n}}$, where b_m denotes the associated mBS. σ_m^2 is the noise power of a mmWave link. The rate of μ Wave and mmWave links are given by the Shannon's formula as $R_j^l = B_l \log_2(1 + \Upsilon_j^l)$, $l \in \{\mu, m\}$, where B_l denotes the subchannel bandwidth of μ Wave or mmWave links.

B. Caching and Computing Model

The probabilities of the service requests of the HMD follow the independent reference model [28], [29] with the request probability $p_j, j \in \mathcal{J}$. Considering all J viewpoints, we have $\sum_{j=1}^J p_j = 1$. μ BSs, mBSs, and HMDs all have caching and computing capabilities. The cache size at μ BSs, mBSs, and HMDs is C^μ , C^m , and C^H , respectively. The caching decision for the MV and SV of the j -th viewpoint is denoted by $y_j^{q,M} \in \{0, 1\}$ and $y_j^{q,S} \in \{0, 1\}$, $q \in \{\mu, m, H\}$. $y_j^{q,\omega} = 1, \omega \in \{M, S\}$ indicates that the MV or SV of the j -th viewpoint is cached at device q , otherwise $y_j^{q,\omega} = 0$. With the cache size constraint, we have $\sum_{j=1}^J d_j^M y_j^{q,M} + d_j^S y_j^{q,S} \leq C^q$.

The computing decisions at μ BSs, mBSs, and HMDs are considered to process the projection and rendering. The CPU-cycle frequency of μ BSs, mBSs, and HMDs is denoted by $f_q, q \in \{\mu, m, H\}$. The average energy consumption constraint of μ BSs, mBSs, and HMDs is denoted by $E_q, q \in \{\mu, m, H\}$. Define ε as the number of computation cycles required to process the projection and rendering of one bit input.

The energy consumed for computing one cycle at μ BSs, mBSs, and HMDs is $k_q = \eta_q f_q^2$, in which η_q is the coefficient related to the hardware architecture indicating the energy efficiency of CPU. The computing decision for the j -th viewpoint is denoted by $z_j^q \in \{0, 1\}$, where $z_j^q = 1$ indicates that the projection is computed at device q , otherwise $z_j^q = 0$. Considering the average energy consumption constraint at device q , we have $\sum_{j=1}^J p_j \varepsilon k_q d_j^M z_j^q \leq E^q$.

In the case where the requested viewpoint cannot be found in HMD cache, μ BS cache or mBS cache, the requested viewpoint is retrieved from the core network through the fiber backhaul

links with an extra backhaul retrieving delay τ_j^r . We assume that the backhaul transmission rate is R_j^b , and the backhaul capacity constraint is B^b .

III. RELIABILITY ANALYSIS OF VR DELIVERY AND PROBLEM FORMULATION

In order to investigate the reliability performance of VR delivery in DC μ Wave-mmWave HetNets, we refer to the reliability defined by 3GPP [30], which is the probability of experiencing an end-to-end latency below the threshold required by the targeted service. Accordingly, using the law of total probability, the reliability of VR delivery can be expressed as,

$$\mathcal{R} = \sum_{j=1}^J p_j \mathbb{P}[\tau_j^\mu < T_j \cup \tau_j^m < T_j], \quad (5)$$

where T_j is the end-to-end latency threshold required by the j -th viewpoint, $\tau_j^l, l \in \{\mu, m\}$ denotes the end-to-end latency when the j -th viewpoint is retrieved over a μ Wave link or mmWave link. Delay contributions to the end-to-end VR delivery latency include the over-the-air transmission delay $\tau_j^{l,t}$, the computing delay $\tau_j^{l,c}$, the sensor sampling delay τ_j^s , the display refresh delay τ_j^d and the backhaul retrieving delay $\tau_j^{l,b}$ if the requested viewpoint is not cached [2]. Thus, when the j -th viewpoint is delivered over a μ Wave link or mmWave link, the end-to-end delay is calculated as

$$\tau_j^l = \tau_j^{l,t} + \tau_j^{l,c} + \tau_j^{l,b} + \tau_j^s + \tau_j^d, \quad j \in \mathcal{J}, l \in \{\mu, m\}. \quad (6)$$

Note that $\tau_j^{l,t}$ is a random variable which is affected by the channel uncertainty of wireless environments and the data size of the delivered viewpoint. The value of $\tau_j^{l,c}$ can be calculated when the caching and computing strategy is determined. Whether the end-to-end delay contains $\tau_j^{l,b}$ depends on whether the requested viewpoint is cached. τ_j^s and τ_j^d are assumed to be constants.

A. Reliability Analysis over DC μ Wave-mmWave HetNets

The reliability of VR delivery is mainly affected by the channel uncertainty of wireless environments. In wireless environments where temporary outages are common due to impairments in SINR, VR's non-elastic traffic behavior poses additional difficulty. Utilizing tools from stochastic geometry, tractable expressions can be obtained to characterize the reliability of VR delivery.

The computing delay $\tau_j^{l,c} = \frac{\varepsilon d_j^M}{f_q}, q \in \{\mu, m, H\}$ when the j -th MV is calculated into SV at device q . Considering the caching and computing strategy for the j -th viewpoint, the computing

delay $\tau_j^{l,c}$ can be expressed as

$$\tau_j^{l,c} = \frac{\varepsilon d_j^M (y_j^{H,M} \| y_j^{l,M}) (z_j^H \| z_j^l)}{z_j^{l,M} f_l + (1 - z_j^{l,M}) f_H}, \quad (7)$$

where $\cdot \| \cdot$ is the logical OR operator. And the backhaul retrieving delay $\tau_j^{l,b}$ can be expressed as

$$\tau_j^{l,b} = (1 - y_j^{l,M} \| y_j^{l,S}) \tau_j^r. \quad (8)$$

Then, we define the over-the-air transmission delay threshold $T_j^{l,t}$ for the j -th viewpoint, which can be calculated as

$$T_j^{l,t} = T_j - \tau_j^{l,c} - \tau_j^{l,b}. \quad (9)$$

The data size of the j -th delivered viewpoint over wireless links also depends on the caching and computing strategy, which can be calculated as

$$D_j^l = y_j^{l,M} z_j^l d_j^S + y_j^{l,M} (1 - z_j^l) d_j^M + y_j^{l,S} d_j^S + (1 - y_j^{l,M}) (1 - y_j^{l,S}) d_j^S, \quad (10)$$

Then, the reliability of delivering the j -th viewpoint over μ Wave or mmWave links is a function of D_j^l and $T_j^{l,t}$, which can be expressed as

$$\mathcal{R}_j^l(D_j^l, T_j^{l,t}) = \mathbb{P}[\tau_j^l < T_j] = \mathbb{P}[\tau_j^{l,t} < T_j^{l,t}] \stackrel{(a)}{=} \mathbb{P}[R_j^l > D_j^l / T_j^{l,t}], l \in \{\mu, m\}, \quad (11)$$

where (a) follows from $\tau_j^{l,t} = D_j^l / R_j^{l,t}$, $D_j^l \in \{d_j^M, d_j^S\}$.

Proposition 1. *When the j -th viewpoint is delivered to the HMD over μ Wave links, the reliability of VR delivery is given as,*

$$\mathcal{R}_j^\mu(D_j^\mu, T_j^{\mu,t}) = \sum_{i=1}^q w_i e^{r_i + \beta_\mu(\nu_j^\mu, r_i)} f_\mu(r_i), \quad (12)$$

where $w_i = \frac{r_i}{(q+1)^2 [L_{q+1}(r_i)]^2}$, r_i is the i -th zero of $L_q(r)$, $L_q(r)$ denotes the Laguerre polynomials, and q is a parameter balancing the accuracy and complexity. $\nu_j^\mu = 2^{\frac{D_j^\mu}{T_j^{\mu,t} B_\mu}} - 1$, $f_\mu(r) = 2\pi\lambda_\mu r e^{-\pi\lambda_\mu r^2}$, $\beta_\mu(\nu_j^\mu, r) = -\nu_j^\mu r^{\alpha_\mu} \sigma_\mu^2 - \pi\lambda_\mu r^2 H_\delta(\nu_j^\mu) + \pi\lambda_\mu s^\delta \Gamma(1 + \delta) \Gamma(1 - \delta)$, $s = \nu_j^\mu r^{\alpha_\mu} P_\mu^{-1}$, $\delta = 2/\alpha_\mu$, $\Gamma(\cdot)$ is the Gamma function, and $H_\delta(x) \triangleq {}_2F_1(1, \delta; 1 + \delta; -x)$ is the Gauss hypergeometric function.

Proof. Please refer to Appendix A. \square

The delivery reliability (12) is in the form of the complementary cumulative distribution

function (CCDF) of SINR over the μ Wave tier. The reliability is monotonically decreasing with the SINR threshold ν_j^μ , which indicates that the reliability increases with the increase of $T_j^{\mu,t}$, while decreases with the increase of D_j^μ .

Proposition 2. *When the j -th viewpoint is delivered to the HMD over mmWave links, the reliability of VR delivery is given as,*

$$\mathcal{R}_j^m(D_j^m, T_j^{m,t}) = \sum_{i=1}^q w_i e^{r_i} \beta_m(\nu_j^m, r_i) f_m(r_i), \quad (13)$$

where $\beta_m(\nu_j^m, r_i) = \sum_{\ell \in \{L, N\}} \rho_\ell(r_i) \sum_{k=1}^{N_\ell} (-1)^{k+1} \binom{N_\ell}{k} e^{-\frac{k\eta_\ell \nu_j^m r_i^{\alpha_\ell} \sigma_m^2}{P_m G}} \mathcal{L}(r_i)$, $\nu_j^m = 2^{\frac{D_j^m}{T_j^{m,t} B_m}} - 1$, $f_m(r) = 2\pi\lambda_m r e^{-\pi\lambda_m r^2}$, $\eta_\ell = N_\ell (N_\ell!)^{-\frac{1}{N_\ell}}$, and

$$\mathcal{L}(r) = \prod_{n \in \{L, N\}} \prod_G \exp \left[-2\pi\lambda_m p_G \sum_{u=1}^{N_n} \binom{N_n}{u} \frac{r^{-\frac{1}{\alpha_n}(u-\frac{2}{\alpha_n})}}{u\alpha_n - 2} {}_2F_1 \left(N_n, u - \frac{2}{\alpha_n}; 1 + u - \frac{2}{\alpha_n}; -sr^{-\frac{1}{\alpha_n}} \right) \right], \quad (14)$$

where p_G is the probability of the random antenna gain defined in (3), and $s = \frac{k\eta_n G \nu_j^m r^{\alpha_n} \sigma_m^2}{M^2 N_n}$.

Proof. Please refer to Appendix B. \square

Taking into consideration the LOS or NLOS channel state, the delivery reliability (13) is the CCDF of SINR over the mmWave tier. Then some remarks can be concluded from Proposition 2.

Remark 1: The reliability of VR delivery over the mmWave tier (13) indicates that the Laplace transform of the interference $\mathcal{L}(r)$ in (14) is independent of the transmit power P_m .

Remark 2: (13) is a monotonically increasing function with respect to $T_j^{m,t}$, and a monotonically decreasing function with respect to D_j^m .

Remark 3: Considering a special case when the viewpoints are only delivered through LOS links, then (13) is a decreasing and convex function with respect to the blockage density κ .

For dual-connectivity μ Wave-mmWave network, according to the addition rule for probability, the delivery reliability for viewpoint j is calculated as

$$\mathcal{R}_j^{DC} = \mathcal{R}_j^\mu(D_j^\mu, T_j^{\mu,t}) + \mathcal{R}_j^m(D_j^m, T_j^{m,t}) - \mathcal{R}_j^\mu(D_j^\mu, T_j^{\mu,t}) \mathcal{R}_j^m(D_j^m, T_j^{m,t}), \quad (15)$$

Note that \mathcal{R}_j^{DC} is the expression of the reliability when the j -th viewpoint is delivered through wireless links. On the other hand, if the MV or SV of the j -th viewpoint is cached in the HMD, we assume that the end-to-end delay is less than the delay threshold with probability 1, i.e., the

reliability is set to 1. Therefore, the complete expression of the reliability can be written as

$$\mathcal{R}_j = \mathbf{1}(y_j^{H,M} \| y_j^{H,S} = 1) + \mathbf{1}(y_j^{H,M} + y_j^{H,S} = 0) \mathcal{R}_j^{DC}, \quad (16)$$

where $\mathbf{1}(\cdot)$ is the indicator function.

B. Link Selection Strategy and Problem Formulation

Since the DC mode is adopted at HMD, it is essential to give the criteria for delivery the viewpoints over the μ Wave link or the mmWave link. In this paper, since the end-to-end delay is the key factor affecting the reliability of VR delivery, we propose the minimum-delay delivery criteria in DC mode as the link selection strategy, which can be written as

$$l_0 = \arg \min_{l \in \{\mu, m\}} \tau_j^l. \quad (17)$$

Proposition 3. *When the j -th viewpoint is not locally cached by the HMD, based on the minimum-delay delivery criteria, the probability that the mmWave link is selected to deliver the viewpoint is given as,*

$$A_j^m = \int_0^\infty p_{\mathcal{R}_j^\mu(D_j^\mu, t)} \mathcal{R}_j^m(D_j^m, (t - \tau_0)^+) dt, \quad (18)$$

where $p_{\mathcal{R}_j^\mu(D_j^\mu, T_j^{\mu,t})} = \frac{\partial \mathcal{R}_j^\mu(D_j^\mu, T_j^{\mu,t})}{\partial T_j^{\mu,t}}$, $\tau_0 = \tau_j^{m,c} + \tau_j^{m,b} - \tau_j^{\mu,c} - \tau_j^{\mu,b}$, and $(\cdot)^+ = \max(\cdot, 0)$.

Proof. According to (17), the delivery probability over mmWave links can be expressed as

$$A_j^m = \mathbb{P}[\tau_j^m < \tau_j^\mu] = \mathbb{P}[\tau_j^{m,t} < \tau_j^{\mu,t} - \tau_0], \quad (19)$$

where $\tau_0 = \tau_j^{m,c} + \tau_j^{m,b} - \tau_j^{\mu,c} - \tau_j^{\mu,b}$. Using the results in Propositions 1 and 2, the cumulative distribution function of $\tau_j^{m,t}$ is directly obtained in (13), and denote the probability density function of (12) with respect to $T_j^{\mu,t}$ as $p_{\mathcal{R}_j^\mu(D_j^\mu, T_j^{\mu,t})} \triangleq \frac{\partial \mathcal{R}_j^\mu(D_j^\mu, T_j^{\mu,t})}{\partial T_j^{\mu,t}}$, we have

$$A_j^m = \int_0^\infty p_{\mathcal{R}_j^\mu(D_j^\mu, T_j^{\mu,t})} \mathcal{R}_j^m(D_j^m, (T_j^{\mu,t} - \tau_0)^+) dT_j^{\mu,t}. \quad (20)$$

□

Accordingly, the probability that the mmWave link is selected to deliver the viewpoint is given as $A_j^m = 1 - A_j^\mu$. Proposition 3 can be used to calculate the expected amount of transmitted data over the μ Wave link and the mmWave link. Thus, the expected number of MVs computed at the μ BS, mBS, and the HMD can be obtained, respectively.

Note that τ_0 represents the difference of the delays (except for the transmission delays) between mmWave links and μ Wave links, where $\tau_j^{l,c}, \tau_j^{l,b}, l \in \{\mu, m\}$ can be calculated by (7) and (8), respectively. From Remark 2, we can deduce that A_j^m is decreasing with τ_0 , which indicates that the caching and computing strategy will have an impact on the delivery probability over mmWave and μ Wave links. For example, if the blockage density in the mmWave tier is low, we can adjust the caching and computing strategy to get a smaller value of τ_0 , thus increasing the delivery probability over mmWave links to improve the reliability of VR delivery.

Remark 4: From Remark 3 and the delivery probability over mmWave links (18), we conclude that when the viewpoints are only delivered through LOS links, A_j^m is a decreasing and convex function with respect to the blockage density κ . In addition, when $\kappa \rightarrow \infty$, we have $A_j^m \rightarrow 0$, and when $\kappa = 0$, $A_j^m < 1$. This indicates that mmWave links cannot be utilized when the blockage density is too high, while μ Wave links can be utilized even if there is no blockage for mmWave links. In other words, μ Wave links can be utilized to enhanced the reliability of VR delivery despite the large mmWave bandwidth.

Next, we can formulate the problem of maximizing the reliability of VR delivery in DC μ Wave-mmWave HetNets by jointly optimizing the caching and computing decision at the μ BS, mBS, and HMD as follow,

$$\mathbf{P1:} \max_{\{y_j^{q,M}, y_j^{q,S}, z_j^q\}} \sum_{j=1}^J p_j \mathcal{R}_j \quad (21a)$$

$$\text{s.t.} \quad \sum_{j=1}^J d_j^M y_j^{q,M} + d_j^S y_j^{q,S} \leq C^q, q \in \{H, \mu, m\}, \quad (21b)$$

$$\sum_{j=1}^J p_j \varepsilon k_H d_j^M (y_j^{H,M} + A_j^{\mu,M} y_j^{\mu,M} + A_j^{m,M} y_j^{m,M}) z_j^H \leq E^H \quad (21c)$$

$$\sum_{j=1}^J p_j \varepsilon A_j^l k_l d_j^M z_j^l \leq E^l, l \in \{\mu, m\}, \quad (21d)$$

$$\sum_{j=1}^J \sum_l A_j^l d_j^S (1 - y_j^{H,M} \|y_j^{H,S}\| \|y_j^{\mu,M}\| \|y_j^{\mu,S}\|) \leq B^b, j \in \mathcal{J}, l \in \{\mu, m\}, \quad (21e)$$

$$y_j^{q,M} \in \{0, 1\}, y_j^{q,S} \in \{0, 1\}, z_j^q \in \{0, 1\}, j \in \mathcal{J}, q \in \{H, \mu, m\}, \quad (21f)$$

where (21a) is the reliability of VR delivery according to (5). (21b) is the cache capacity constraint. (21c) is the average computing energy consumption at the HMD. (21d) is the average computing energy consumption at the μ BS or mBS. (21e) is the backhaul bandwidth constraint, and (21f) ensures the binary decision of the caching and computing decision.

C. Problem Reformulation

Problem **P1** is difficult to solve because the objective function (21a) and the constraint (21e) contain logical operations. Fortunately, we can explore the coupling relationship between the caching and computing strategies to greatly reduce the solution space.

Lemma 1. *For any viewpoint $j \in \mathcal{J}$, the following caching and computing relationships hold,*

- 1) $(y_j^{H,M} \| y_j^{H,S}) + (y_j^{\mu,M} \| y_j^{\mu,S} \| y_j^{m,M} \| y_j^{m,S}) \leq 1$,
- 2) $y_j^{q,M} + y_j^{q,S} \leq 1$, $q \in \{\mu, m, H\}$,
- 3) if $y_j^{l,M} = 1$, then $z_j^l + z_j^H = 1$ holds, $l \in \{\mu, m\}$.

Proof. 1) means that the HMD and the MEC server (at the μ BS or mBS) should not cache the j -th viewpoint simultaneously. This is because when the j -th viewpoint is cached at the HMD, the reliability is set to 1, thus there is no need to cache it at the MEC server.

2) means that there is no need to cache the MV and the SV of the j -th viewpoint simultaneously at the HMD or the MEC server. This is because the caching and the computing strategy is determined before delivering the j -th viewpoint, and caching MV or SV is two different strategies, which should not exist simultaneously.

3) holds because when the MV of the j -th viewpoint is cached at the μ BS or mBS, it should be computed either at the MEC server or at the HMD. On the other hand, the computing strategy over the μ Wave link can be different from that over the mmWave link. \square

According to Lemma 1, the caching and computing strategies are coupled, which can be used to reduce the solution space to 18 joint caching and computing strategies for the j -th viewpoint, which are listed in Table I. In Table I, we rewrite the joint caching and computing strategies of the j -th viewpoint in the form of 9-tuple as $[y_j^{H,M} \ y_j^{H,S} \ z_j^H, y_j^{\mu,M} \ y^{\mu,S} \ z^{\mu}, y_j^{m,M} \ y^{m,S} \ z^m]$. To distinguish whether the MVs computed at the HMD is cached locally, or cached at μ BSs or mBSs, we further rewrite z_j^H as $z_j^H \triangleq (z_j^{H(H)} z_j^{H(\mu)} z_j^{H(m)})$.

The 18 joint caching and computing strategies can be divided into 4 types based on different caching strategies, i.e., local caching, caching at μ BSs and mBSs simultaneously, caching at μ BSs or mBSs, and backhaul retrieving. In each type, different computing strategies are included. Detailed descriptions are as follows,

- **Local caching (Strategy 1, 2):** In this type, the viewpoint j is cached locally at the HMD, i.e. $y_j^{H,M} = 1$, or $y_j^{H,S} = 1$. Since over-the-air transmission and backhaul retrieving are not required in this case, the viewpoint j can be guaranteed to be obtained in time, so the

delivery reliability is set to 1. When $y_j^{H,M} = 1$, the j -th MV is cached locally, at the cost of d_j^M cache size and $k_H d_j^M \varepsilon$ computing energy consumption. When $y_j^{H,S} = 1$, the j -th SV is directly obtained locally, at the cost of d_j^S cache size.

- **Caching at μ BSs and mBSs simultaneously:** In this type, depending on whether the MV or SV of the j -th viewpoint is cached at μ BSs and mBSs, 4 cases can be generated,

- **(Strategy 3 – 6)** The j -th MV is cached at both μ BSs and mBSs. The delivery reliability over the μ Wave link is $\mathcal{R}_j^\mu(d_j^S, T_j - \frac{\varepsilon d_j^M}{f_\mu})$ when the MV is projected into SV at the μ BS, and $\mathcal{R}_j^\mu(d_j^M, T_j - \frac{\varepsilon d_j^M}{f_H})$ when the MV is projected into SV at the HMD. Likewise, the delivery reliability over the mmWave link is $\mathcal{R}_j^m(d_j^S, T_j - \frac{\varepsilon d_j^M}{f_m})$ when the MV is projected into SV at the mBS, and $\mathcal{R}_j^m(d_j^M, T_j - \frac{\varepsilon d_j^M}{f_H})$ when the MV is projected into SV at the HMD. The computing energy consumption is $A_{q_1} k_{q_2} d_j^M \varepsilon$, $q_1 \in \{\mu, m\}$, $q_2 \in \{\mu, m, H\}$ at the μ BS, mBS or HMD for strategy 3, 4, 5, and $k_v d_j^M \varepsilon$ at the HMD for strategy 6.
- **(Strategy 7, 8)** The MV is cached at μ BSs, and the SV is cached at mBSs. The delivery reliability over the μ Wave link depends on the computing strategy similar to the case in strategy 3 – 6. The delivery reliability over the mmWave link is $\mathcal{R}_j^m(d_j^S, T_j)$. The computing energy consumption is $A_\mu k_q d_j^M \varepsilon$, $q \in \{\mu, v\}$ at the μ BS or HMD.
- **(Strategy 9, 10)** The SV is cached at μ BSs, and the MV is cached at mBSs. The delivery reliability over the μ Wave link is $\mathcal{R}_j^\mu(d_j^S, T_j)$. The delivery reliability over the mmWave link depends on the computing strategy similar to the case in strategy 3 – 6. The computing energy consumption is $A_m k_q d_j^M \varepsilon$, $q \in \{m, v\}$ at the mBS or HMD.
- **(Strategy 11)** The SV is cached at both μ BSs and mBSs. The delivery reliability over the μ Wave link is $\mathcal{R}_j^\mu(d_j^S, T_j)$, and that over the mmWave link is $\mathcal{R}_j^m(d_j^S, T_j)$. The cost of cache size is d_j^S at both μ BSs and mBSs, without computing energy consumption.

- **Caching at μ BSs or mBSs:** In this type, depending on whether the MV or SV is cached at μ BSs or mBSs, 4 cases can be generated,

- **(Strategy 12, 13)** The MV is cached at μ BSs. The delivery reliability over the μ Wave link depends on the computing strategy similar to the case in strategy 3 – 6. Considering the backhaul retrieve delay, the delivery reliability over the mmWave link is $\mathcal{R}_j^m(d_j^S, T_j - \tau_j^r)$. The computing energy consumption is $A_\mu k_q d_j^M \varepsilon$, $q \in \{\mu, v\}$ at the μ BS or HMD, and the backhaul cost is $A_m d_j^S$.
- **(Strategy 14)** The SV is cached at μ BSs. The delivery reliability over the μ Wave link is $\mathcal{R}_j^\mu(d_j^S, T_j)$, and that over the mmWave link is $\mathcal{R}_j^m(d_j^S, \tau_j^r)$. No computing delay or

TABLE I
JOINT CACHING AND COMPUTING STRATEGY IN DC μ WAVE-MMWAVE HETNETS

Type	Strategy Index k	Joint Decision	μWave Link		mmWave Link		Caching Occupancy ξ_{jk}^q			Computing Energy Consumption ζ_{jk}^q			Backhaul Cost φ_{jk}
			D_j^μ	$\tau_j^{\mu,c} + \tau_j^{\mu,b}$	D_j^m	$\tau_j^{m,c} + \tau_j^{m,b}$	μBS	mBS	HMD	μBS	mBS	HMD	
Local Caching	1	[10(000),000,000]	–	–	–	–	0	0	d_j^M	0	0	$k_H d_j^M \varepsilon$	0
	2	[01(000),000,000]	–	–	–	–	0	0	d_j^S	0	0	0	0
Caching at μ BSs and mBSs simultaneously	3	[00(000),101,101]	d_j^S $\frac{\varepsilon d_j^M}{f_m}$	d_j^S $\frac{\varepsilon d_j^M}{f_m}$	d_j^M $\frac{\varepsilon d_j^M}{f_m}$	d_j^M $\frac{\varepsilon d_j^M}{f_m}$	0	$A_\mu k_\mu d_j^M \varepsilon$	$A_m k_m d_j^M \varepsilon$	0	$A_m k_m d_j^M \varepsilon$	0	0
	4	[00(001),101,100]	d_j^S $\frac{\varepsilon d_j^M}{f_m}$	d_j^M $\frac{\varepsilon d_j^M}{f_m}$	d_j^M $\frac{\varepsilon d_j^M}{f_m}$	d_j^M $\frac{\varepsilon d_j^M}{f_m}$	0	$A_\mu k_\mu d_j^M \varepsilon$	0	$A_m k_m d_j^M \varepsilon$	0	$A_m k_H d_j^M \varepsilon$	0
	5	[00(010),100,101]	d_j^M $\frac{\varepsilon d_j^M}{f_m}$	d_j^S $\frac{\varepsilon d_j^M}{f_m}$	d_j^M $\frac{\varepsilon d_j^M}{f_m}$	d_j^M $\frac{\varepsilon d_j^M}{f_m}$	0	0	0	$A_m k_m d_j^M \varepsilon$	$A_\mu k_H d_j^M \varepsilon$	0	0
	6	[00(011),100,100]	d_j^M $\frac{\varepsilon d_j^M}{f_m}$	d_j^M $\frac{\varepsilon d_j^M}{f_m}$	d_j^M $\frac{\varepsilon d_j^M}{f_m}$	d_j^M $\frac{\varepsilon d_j^M}{f_m}$	0	0	0	0	0	$k_H d_j^M \varepsilon$	0
	7	[00(000),101,010]	d_j^S $\frac{\varepsilon d_j^M}{f_m}$	d_j^S $\frac{\varepsilon d_j^M}{f_m}$	0	d_j^M $\frac{\varepsilon d_j^M}{f_m}$	d_j^S $\frac{\varepsilon d_j^M}{f_m}$	0	$A_\mu k_\mu d_j^M \varepsilon$	0	0	0	0
	8	[00(010),100,010]	d_j^M $\frac{\varepsilon d_j^M}{f_m}$	d_j^S $\frac{\varepsilon d_j^M}{f_m}$	0	d_j^M $\frac{\varepsilon d_j^M}{f_m}$	d_j^S $\frac{\varepsilon d_j^M}{f_m}$	0	0	0	0	$A_\mu k_H d_j^M \varepsilon$	0
	9	[00(000),010,101]	d_j^S $\frac{\varepsilon d_j^M}{f_m}$	0	d_j^S $\frac{\varepsilon d_j^M}{f_m}$	d_j^M $\frac{\varepsilon d_j^M}{f_m}$	d_j^S $\frac{\varepsilon d_j^M}{f_m}$	0	0	0	$A_m k_m d_j^M \varepsilon$	0	0
	10	[00(001),010,100]	d_j^S $\frac{\varepsilon d_j^M}{f_m}$	0	d_j^M $\frac{\varepsilon d_j^M}{f_m}$	d_j^S $\frac{\varepsilon d_j^M}{f_m}$	d_j^M $\frac{\varepsilon d_j^M}{f_m}$	0	0	0	0	$A_m k_H d_j^M \varepsilon$	0
	11	[00(000),010,010]	d_j^S $\frac{\varepsilon d_j^M}{f_m}$	0	d_j^S $\frac{\varepsilon d_j^M}{f_m}$	0	d_j^S $\frac{\varepsilon d_j^M}{f_m}$	0	0	0	0	0	0
Caching at μ BSs or mBSs	12	[00(000),101,000]	d_j^S $\frac{\varepsilon d_j^M}{f_m}$	d_j^S $\frac{\varepsilon d_j^M}{f_m}$	τ_j^r d_j^M	d_j^M $\frac{\varepsilon d_j^M}{f_m}$	0	0	$A_\mu k_\mu d_j^M \varepsilon$	0	0	$A_m d_j^S$	
	13	[00(010),100,000]	d_j^M $\frac{\varepsilon d_j^M}{f_m}$	d_j^S $\frac{\varepsilon d_j^M}{f_m}$	τ_j^r d_j^M	d_j^M $\frac{\varepsilon d_j^M}{f_m}$	0	0	0	0	0	$A_\mu k_H d_j^M \varepsilon$	$A_m d_j^S$
	14	[00(000),010,000]	d_j^S $\frac{\varepsilon d_j^M}{f_m}$	0	d_j^S $\frac{\varepsilon d_j^M}{f_m}$	τ_j^r d_j^S	d_j^S $\frac{\varepsilon d_j^M}{f_m}$	0	0	0	0	0	$A_m d_j^S$
	15	[00(001),000,100]	d_j^S $\frac{\varepsilon d_j^M}{f_m}$	τ_j^r d_j^M	d_j^M $\frac{\varepsilon d_j^M}{f_m}$	0	d_j^M $\frac{\varepsilon d_j^M}{f_m}$	0	0	0	0	$A_m k_H d_j^M \varepsilon$	$A_\mu d_j^S$
	16	[00(000),000,101]	d_j^S $\frac{\varepsilon d_j^M}{f_m}$	τ_j^r d_j^S	d_j^S $\frac{\varepsilon d_j^M}{f_m}$	0	d_j^M $\frac{\varepsilon d_j^M}{f_m}$	0	0	$A_m k_m d_j^M \varepsilon$	0	$A_\mu d_j^S$	
	17	[00(000),000,010]	d_j^S $\frac{\varepsilon d_j^M}{f_m}$	τ_j^r d_j^S	0	0	d_j^S $\frac{\varepsilon d_j^M}{f_m}$	0	0	0	0	0	$A_\mu d_j^S$
Backhaul Retrieving	18	[00(000),000,000]	d_j^S $\frac{\varepsilon d_j^M}{f_m}$	τ_j^r d_j^S	τ_j^r d_j^S	0	0	0	0	0	0	0	d_j^S

computing energy consumption is generated, and the backhaul cost is $A_m d_j^S$.

- **(Strategy 15, 16)** The MV is cached at mBSs. Considering the backhaul delay, the delivery reliability over the μ Wave link is $\mathcal{R}_j^\mu(d_j^S, T_j - \tau_j^r)$. The delivery reliability over the mmWave link depends on the computing strategy similar to the case in strategy 3 – 6. The computing energy consumption is $A_m k_q d_j^M \varepsilon, q \in \{m, v\}$ at the mBS or HMD, and the backhaul cost is $A_\mu d_j^S$.
- **(Strategy 17)** The SV is cached at mBSs. The delivery reliability over the μ Wave link is $\mathcal{R}_j^\mu(d_j^S, T_j - \tau_j^r)$, and that over the mmWave link is $\mathcal{R}_j^m(d_j^S, T_j)$. No computing delay or computing energy consumption is generated, and the backhaul cost is $A_\mu d_j^S$.
- **Backhaul Retrieve (Strategy 18):** The delivery reliability over the μ Wave link is $\mathcal{R}_j^\mu(d_j^S, T_j - \tau_j^r)$, and that over the mmWave link is $\mathcal{R}_j^m(d_j^S, T_j - \tau_j^r)$. The viewpoint j is retrieved via the backhaul at the cost of d_j^S .

Denote k as the strategy index of the 18 strategies listed in Table I, and $x_{jk} \in \{0, 1\}$ as the binary decision variable for the strategy of the j -th viewpoint. For the k -th strategy, the corresponding caching occupancy, computing energy consumption and the backhaul cost is denoted as $\xi_{jk}^q, \zeta_{jk}^q, q \in \{\mu, m, H\}$, and φ_{jk} , respectively. Then problem **P1** can be reformulated as a multiple-choice multi-dimension knapsack problem (MMKP) as follows,

$$\mathbf{P2:} \max_{\{x_{jk}\}, j \in \mathcal{J}, k \in \{1, 2, \dots, 18\}} \sum_{j=1}^J \sum_{k=1}^{18} p_j \mathcal{R}_{jk} x_{jk} \quad (22a)$$

$$\text{s.t.} \quad \sum_{j=1}^J \sum_{k=1}^{18} \xi_{jk}^q x_{jk} \leq C^q, q \in \{H, \mu, m\}, \quad (22b)$$

$$\sum_{j=1}^J \sum_{k=1}^{18} p_j \zeta_{jk}^q x_{jk} \leq E^q, q \in \{H, \mu, m\}, \quad (22c)$$

$$\sum_{j=1}^J \sum_{k=1}^{18} \varphi_{jk} x_{jk} \leq B^b, \quad (22d)$$

$$\sum_{k=1}^{18} x_{jk} = 1, j \in \mathcal{J}, \quad (22e)$$

$$x_{jk} \in \{0, 1\}, j \in \mathcal{J}, k \in \{1, 2, \dots, 18\}. \quad (22f)$$

Problem **P2** is a 18-choice 7-dimensional MMKP problem, which is proved to be NP-hard. Specifically, J viewpoints are considered as J classes, while the 18 joint caching and computing strategies belonging to each class j are considered as 18 items. The problem is to choose one item from each class such that the profit sum is maximized while satisfying the capacity and energy consumption constraints.

IV. OPTIMIZATION OF JOINT CACHING AND COMPUTING

A. Optimal solution using BFBB algorithm

We propose a best-first branch and bound (BFBB) algorithm to solve the MMKP problem **P2**. The key idea of the BFBB algorithm can be described as follows: 1) Compute upper bounds and lower bounds of the optimal solution and discard branches that cannot produce a better solution than the best one found so far by the algorithm; 2) Utilize a priority queue to select the node with the highest priority as the expanded node of the search tree.

1) *Computation of upper and lower bound*: First, to compute the upper bound of problem **P2**, we construct an auxiliary problem **P3**, which relaxes the constraints into the sum of constraints (22b)–(22d) as follows,

$$\mathbf{P3:} \max_{\{x_{jk}\}} \sum_{j=1}^J \sum_{k \in \mathcal{K}} p_j \mathcal{R}_{jk} x_{jk} \quad (23a)$$

$$\text{s.t.} \quad \sum_{j=1}^J \sum_{k \in \mathcal{K}} \varpi_{jk} x_{jk} \leq C_0, \quad (23b)$$

$$(22e), (22f),$$

where $\varpi_{jk} = \left(\varphi_{jk} + \sum_{q \in \{H, \mu, m\}} (\xi_{jk}^q + p_j \zeta_{jk}^q) \right)$ and $C_0 = B^b + \sum_{q \in \{H, \mu, m\}} (C^q + E^q)$.

For each viewpoint j , select the joint caching and computing decision k which maximizes $\frac{\mathcal{R}_{jk}}{\varpi_{jk}}$, and denote the corresponding decision as k_{\max} for each viewpoint j . Let \mathcal{R}_{UB} denote the upper bound of problem **P3**, and let $\varpi_0 = \sum_{j \in \mathcal{J}} \varpi_{jk_{\max}}$, $\mathcal{R}_0 = \sum_{j \in \mathcal{J}} \mathcal{R}_{jk_{\max}}$, then there exist the following two cases,

- $\varpi_0 > C_0$. In this case, the solution of problem **P3** is upper bounded by

$$\mathcal{R}_{\text{UB}} = \sum_{j \in \mathcal{J}} \mathcal{R}_{jk_{\max}} \times \left(\frac{C_0}{\sum_{j \in \mathcal{J}} \varpi_{jk_{\max}}} \right). \quad (24)$$

- $\varpi_0 < C_0$. In this case, the constraint (23b) is not violated when decision $x_{jk_{\max}}$ is selected for all $j \in \mathcal{J}$. The remaining items are merged into the same class L , with items indexed by $\ell = 1, \dots, N_f$. The remaining items are sorted in descending order of $\frac{\mathcal{R}_\ell}{\varpi_\ell}$. Then, the problem is converted into choosing the remaining items with the remaining capacity constraint equals to $C_0 - \varpi_0$. Adopting greedy algorithm, we select the items in descending order of $\frac{\mathcal{R}_\ell}{\varpi_\ell}$ to fill the remaining capacity until the capacity constraint is violated. In particular, denote $\hat{\ell} \in [1, \ell]$ the index of the item that violates the remaining capacity constraint $C_0 - \varpi_0$, which can be defined as,

$$\hat{\ell} = \min \left\{ \hat{\ell} : \sum_{\ell=1}^{\hat{\ell}-1} \varpi_\ell \leq C_0 - \varpi_0 < \sum_{\ell=1}^{\hat{\ell}} \varpi_\ell \right\}. \quad (25)$$

Then the solution of problem **P3** is upper bounded by

$$\mathcal{R}_{\text{UB}} = \mathcal{R}_0 + \sum_{\ell=1}^{\hat{\ell}-1} \mathcal{R}_\ell + \left(\frac{(C_0 - \varpi_0) - \sum_{\ell=1}^{\hat{\ell}-1} \varpi_\ell}{\varpi_q} \right) \times \mathcal{R}_{\hat{\ell}}. \quad (26)$$

Lemma 2. \mathcal{R}_{UB} is an upper bound for the auxiliary problem **P3** as well as the problem **P2**.

Proof. The proof can be shown by contradiction for the first case ($\varpi_0 > C_0$) of this lemma. Suppose that there exists a solution $\hat{X} = (\hat{x}_{1k_1}, \dots, \hat{x}_{jk_j}, \dots, \hat{x}_{Jk_J})$ satisfying problem **P3** with corresponding objective value $\hat{\mathcal{R}} = \sum_{j \in \mathcal{J}} \mathcal{R}_{jk_j}$ such that $\mathcal{R}_0 \times \left(\frac{C_0}{\varpi_0} \right) < \hat{\mathcal{R}}$. Then we have $\frac{\mathcal{R}_0}{\varpi_0} < \frac{\hat{\mathcal{R}}}{C_0}$. Since $\hat{\varpi} = \sum_{j \in \mathcal{J}} \varpi_{jk_j} \leq C_0$, we have $\frac{\hat{\mathcal{R}}}{C_0} \leq \frac{\hat{\mathcal{R}}}{\hat{\varpi}}$. Thus $\frac{\mathcal{R}_0}{\varpi_0} < \frac{\hat{\mathcal{R}}}{\hat{\varpi}}$.

According to the descending order of $\frac{\mathcal{R}_{jk}}{\varpi_{jk}}$, the inequality $\frac{\mathcal{R}_{jk_{\max}}}{\varpi_{jk_{\max}}} \geq \frac{\mathcal{R}_{jk_j}}{\varpi_{jk_j}}$, $\forall j \in \mathcal{J}$ holds, thus we have

$$\frac{\sum_{j \in \mathcal{J}} \mathcal{R}_{jk_{\max}}}{\sum_{j \in \mathcal{J}} \varpi_{jk_{\max}}} \geq \frac{\sum_{j \in \mathcal{J}} \mathcal{R}_{jk_j}}{\sum_{j \in \mathcal{J}} \varpi_{jk_j}}, \quad (27)$$

which is contradictory to $\frac{\mathcal{R}_{\max}}{\varpi_{\max}} < \frac{\hat{\mathcal{R}}}{\hat{\varpi}}$.

For the second case ($\varpi_0 \leq C_0$), the remaining capacity is filled with the remaining items as

a knapsack problem, so the upper bound can be obtained also by the greedy algorithm.

Since problem **P3** is a relaxed problem of the problem **P2**, it is obvious that UB is an upper bound for **P2**. □

To determine an initial feasible solution that can be used as the starting lower bound, we develop a heuristic algorithm for obtaining the lower bound of problem **P2** as described in Algorithm 1. The algorithm is based on the conception of aggregate resource saving [31] considering the multiple resource constraints in **P2**. Specifically, the solutions for each viewpoint that achieve lowest reliability is selected as initial solution. The solution is then upgraded by choosing a new solution for a viewpoint which has the maximum aggregate resource saving while increasing the objective function of total reliability. The aggregate resource saving is defined as

$$\Delta\varpi_{jk} = \varpi_{j\rho[j]} - \varpi_{jk}. \quad (28)$$

Note that there might be some solutions that violate the constraints but achieve higher reliability. To obtain a tighter lower bound, we downgrade some of the solutions to get a feasible solution, which may increase the total value of reliability.

2) *Best-first principle of priority*: The candidate nodes to be expanded are stored in the priority queue, and assume that the level of the search tree where a candidate node is located is denoted as j_0 . Define the best-first principle of priority as the maximum upper bounds of the candidate nodes, which can be calculated as

$$\mathcal{P} = \sum_{j=1}^{j_0} p_j \mathcal{R}_{jk_j} x_{jk_j} + \tilde{\mathcal{R}}_{\text{UB}}, \quad (29)$$

where $\tilde{\mathcal{R}}_{\text{UB}}$ is the upper bound of the remaining capacity constraint problem of a candidate node as follows,

$$\mathbf{P4:} \max_{\{x_{jk}\}} \sum_{j=j_0+1}^J \sum_{k \in \mathcal{K}} p_j \mathcal{R}_{jk} x_{jk} \quad (30a)$$

$$\text{s.t.} \quad \sum_{j=j_0+1}^J \sum_{k \in \mathcal{K}} \varpi_{jk} x_{jk} \leq C_0 - \sum_{j=1}^{j_0} \sum_{k \in \mathcal{K}} \varpi_{jk_j} x_{jk_j}, \quad (30b)$$

(22e), (22f).

The best-first principle of priority \mathcal{P} is the sum of the current reliability value of a candidate node and its remaining possible reliability value, i.e., the upper bound of problem **P4**. Note that

Algorithm 1: Heuristic Lower Bound Computation Algorithm

Input: $\mathcal{P}_s, F, C, \epsilon$;
Output: Optimal solution $\mathbf{p}^* = (p_i^*)_{i \in \mathcal{F}}$;

- 1 **initialization:** ;
- 2 Select the lowest-valued solution for each viewpoint.
- 3 Replace a strategy of a viewpoint which has the highest positive value of $\Delta\varpi_{jk}$ and subject to the resource constraints (22b)–(22d). If no such strategy is found, then a strategy with the highest $\Delta\mathcal{R}_{jk}/\Delta\varpi_{jk}$;
- 4 **if** no such solution is found in step 3 **then**
- 5 | go to step 8;
- 6 **else**
- 7 | look for another solution in step 3;
- 8 **if** there exist higher-valued solutions than the selected solution for any viewpoint **then**
- 9 | select a highest-valued strategy \mathcal{R}_{jk} with the minimum aggregate resource consumption ϖ_{jk} ;
- 10 Replace a lower-valued strategy \mathcal{R}_{jk} that consumes the maximum aggregate resource ϖ_{jk} with the strategy selected in step 9;
- 11 **if** a solution is found in step 10 **then**
- 12 | **if** the solution satisfies the constraints (22b)–(22d) **then**
- 13 | | look for a better solution in step 3;
- 14 | **else**
- 15 | | go to step 10 for another downgrade.
- 16 **else**
- 17 | revive the solution obtained at the end of step 3 and terminate.

the form of problem **P4** is the same as that of problem **P3**, thus the upper bound of problem **P4** can be obtained using the similar method described in Lemma 2.

The advantage of applying the best-first principle of priority is that the first obtained feasible solution using the branch and bound searching method achieves the maximum value of reliability of VR delivery, which accelerates the searching process to make it faster to find the optimal solution.

3) *The proposed BFBB algorithm:* In this subsection, we propose the optimal joint caching and computing solution based on BFBB algorithm to solve problem **P2**, as described in Algorithm 2. The BFBB algorithm starts by initializing 18 strategies of the first viewpoint into the priority queue, and using Algorithm 1 to obtain the lower bound of the solution. The next node to be expanded is selected according to the best-first principle of priority (29), and the lower bound is then updated by directly computing the solution of $\mathbf{x}_{j_0 k_{j_0}}$. To perform the branch and bound operation, the feasibility of the expanded child node is verified, and the upper bound of the extended child node is computed using (29). To accelerate the searching process, the lower

bound \mathcal{R}_{LB} is updated using Algorithm 1 in step 13, thus more branches of the search tree can be pruned in step 11. The optimality of the BFBB algorithm is guaranteed by the best-first principle. Since the nodes added into the PQ all correspond to feasible solutions, when $j_0 = J$, i.e., at step 5, the algorithm obtains the biggest value such that \mathbf{x}_{Jk_J} is feasible. Then \mathbf{x}_{Jk_J} is the optimal solution for problem **P2**.

Algorithm 2: The Optimal Joint Caching and Computing Solution based on BFBB

Input: $p_j, \mathcal{R}_{jk}, \xi_{jk}^q, \zeta_{jk}^q, \varphi_{jk}^q, C^q, E^q, B^b, j \in \mathcal{J}, k \in \mathcal{K}, q \in \{H, \mu, m\}$;
Output: Optimal solution $\{\mathbf{x}_{jk}^*\}, j \in \mathcal{J}, k \in \mathcal{K}$;

1 **initialization:** Using Algorithm 1 to obtain the lower bound of the solution \mathcal{R}_{LB} ; denote the priority queue as PQ;

2 **while** $\text{PQ} \neq \emptyset$ **do**

3 Select a node $\mathbf{x}_{j_0 k_{j_0}} \triangleq \{x_{1k_1}, x_{2k_2}, \dots, x_{j_0 k_{j_0}}\}$ from PQ according to the best-first principle of priority (29), and remove $\mathbf{x}_{j_0 k_{j_0}}$ from PQ;

4 Update the lower bound of the solution \mathcal{R}_{LB} using $\mathbf{x}_{j_0 k_{j_0}}$;

5 **if** $j_0 = J$ **then**

6 Exit the loop with the optimal solution \mathbf{x}_{Jk_J} ;

7 Expand the node $\mathbf{x}_{j_0 k_{j_0}}$ to obtain its child nodes \mathbb{C} ;

8 **while** $\mathbb{C} \neq \emptyset$ **do**

9 **if** $\mathbf{x}_{(j_0+1)k}$ corresponds to a feasible solution **then**

10 Calculate the upper bound of the solution \mathcal{R}_{UB} containing $\mathbf{x}_{(j_0+1)k}$ using (29);

11 **if** $\mathcal{R}_{UB} > \mathcal{R}_{LB}$ **then**

12 add $\mathbf{x}_{(j_0+1)k}$ into PQ;

13 Update the current maximum value of \mathcal{R}_{LB} using Algorithm 1;

B. Suboptimal solution based on DCP

In this subsection, a suboptimal solution for solving **P2** is proposed by using difference of convex programming (DCP) with lower computation complexity. First, we equivalently transform **P2** into a continuous optimization problem, which can be written as,

$$\mathbf{P5:} \min_{\{x_{jk}\}} \sum_{j \in \mathcal{J}} \sum_{k \in \mathcal{K}} -p_j \mathcal{R}_{jk} x_{jk} \quad (31a)$$

$$\text{s.t. } 0 \leq x_{jk} \leq 1, j \in \mathcal{J}, k \in \mathcal{K}, \quad (31b)$$

$$\sum_{j \in \mathcal{J}} \sum_{k \in \mathcal{K}} x_{jk} (1 - x_{jk}) \leq 0, \quad (31c)$$

$$(22b), (22c), (22d), (22e),$$

where the binary variable constraint (22f) in **P2** is substituted by continuous variable constraints (31b) and (31c). Thus, by solving the continuous optimization problem **P5**, the computation complexity is greatly reduced compared with that by directly solving **P2**. Nevertheless, the constraint (31c) is a concave function instead of a convex function, which becomes the main difficulty for solving **P5**.

Algorithm 3: Suboptimal solution based on DCP

Initialize: counter $i = 0$, obtain an initial feasible solution $\{x_{jk}^0\}$ using Algorithm 1, threshold $\epsilon = 10^{-5}$;

repeat

Compute: $\hat{f}(\mathbf{x}; \mathbf{x}^i) \triangleq f(\mathbf{x}^i) + \nabla f(\mathbf{x}^i)^T(\mathbf{x} - \mathbf{x}^i)$.

Solve: Set the value of $\{x_{jk}^{i+1}\}$ to be a solution of the following convex problem:

$$\begin{aligned} \min_{\{x_{jk}\}} \quad & f_0(\{x_{jk}\}) - \phi \hat{f}(\{x_{jk}\}; \{x_{jk}^i\}) \\ \text{s.t.} \quad & (22b), (22c), (22d), (22e), (31b). \end{aligned}$$

 where $f_0(\{x_{jk}\}) = \sum_{j \in \mathcal{J}} \sum_{k \in \mathcal{K}} -p_j \mathcal{R}_{jk} x_{jk}$.

Update: $i \leftarrow i + 1$, $\{x_{jk}^i\} \leftarrow \{x_{jk}^{i-1}\}$;

until $(f_0(\mathbf{x}^{i-1}) - \phi f(\mathbf{x}^{i-1})) - (f_0(\mathbf{x}^i) - \phi f(\mathbf{x}^i)) \leq \epsilon$;

To tackle this difficulty, we utilize a penalty function to bring the concave constraint into the objective function, which can be written as,

$$\begin{aligned} \mathbf{P6:} \quad & \min_{\{x_{jk}\}} \quad \sum_{j \in \mathcal{J}} \sum_{k \in \mathcal{K}} -p_j \mathcal{R}_{jk} x_{jk} - \phi f(\mathbf{x}) \\ \text{s.t.} \quad & (22b), (22c), (22d), (22e), (31b), \end{aligned} \tag{32a}$$

where ϕ is a penalty parameter and $\phi > 0$, $f(\mathbf{x}) = \sum_{j \in \mathcal{J}} \sum_{k \in \mathcal{K}} x_{jk}(x_{jk} - 1)$. To ensure the equivalence between **P5** and **P6**, according to [32], ϕ should satisfy,

$$\phi > \frac{-p_j \mathcal{R}_{jk} x_{jk}^0 - g(0)}{\phi_0}, \tag{33}$$

where x_{jk}^0 denotes any feasible solution, $g(\phi)$ denotes the optimal objective value for **P6**, and $\phi_0 = \min_{\mathbf{x}} \{\sum_{j \in \mathcal{J}} \sum_{k \in \mathcal{K}} x_{jk}(1 - x_{jk}) : (22b), (22c), (22d), (22e), (31b)\}$.

Note that the objective function in **P6** is in the form of a difference of two convex functions. Therefore, we adopt DCP to solve this problem as outlined in Algorithm 3. Specifically, the objective function is convexified by the linearization of the second term $f(\mathbf{x})$ in step 3. The complexity of Algorithm 3 lies in solving a series of convex problems in steps 3-6. These convex problems can be solved using the polynomial interior point method [33], which requires

TABLE II
PARAMETER VALUES

Parameters	Physical meaning	Values
P_μ / P_m	Transmit power of μ BSs / mBSs	30 dBm / 30 dBm
B_μ / B_m	Bandwidth assigned to each user at μ Wave / mmWave	100 MHz / 500 MHz
α_L / α_N	Path loss exponent of LoS and NLoS	2.5 / 4
θ	Mainlobe beamwidth	30°
M/m	Mainlobe antenna gain / sidelobe antenna gain	10 dB / -10 dB
κ	Blockage density	6×10^{-4} (Unless otherwise stated)
N_L/N_N	Nakagami fading parameter for LoS and NLoS channel	3 / 2
λ_μ / λ_m	density of μ BSs / mBSs	$10^{-5} / 3 \times 10^{-5}$ nodes/m ²
T_j	End-to-end delay threshold	20 ms (Unless otherwise stated)
δ	Skewness of the viewpoint popularity	0.8
J	The number of viewpoints	20
D_j^M / D_j^S	Size of MVs / SVs	1 Mb / 3 Mb
ε	The number of computation cycles required for 1 bit input	10
$f_H / f_\mu / f_m$	CPU cycle of HMDs / μ BSs / mBSs	$10^9 / 3 \times 10^9 / 3 \times 10^9$
$\eta_H / \eta_\mu / \eta_m$	Energy efficiency coefficient of HMDs / μ BSs / mBSs	$10^{-25} / 10^{-26} / 10^{-26}$
τ_j^r	Backhaul retrieving delay	10 ms

a third degree polynomial complexity in terms of the number of variables. Let L be the total number of iterations, then the complexity of Algorithm 3 is $\mathcal{O}(L(JK)^3)$, where J is the number of viewpoints, and K is the number of strategies for the j -th viewpoint.

V. PERFORMANCE EVALUATION

In this section, the performances of the proposed BFBB and DCP algorithms are evaluated through numerical results. The default parameter values of network environment, mobile edge resources and VR videos are listed in Table II. For comparison, four benchmark algorithms are provided as follows,

- Local SV caching (LSC): First, the SVs are cached locally at the HMD according to the descending order of the popularity of the viewpoints until the caching capacity is full. Then, the remaining SVs are cached at μ BSs and mBSs according to the descending order of the popularity until the caching capacities are full. Then the remaining viewpoints are delivered via the backhaul.
- Local computing with MV caching preferentially (LC-MCP): The MVs are cached at the HMD according to the descending order of the popularity of the viewpoints until the local computing resources are fully utilized. If there remains caching capacity, the SVs are cached until the caching capacity is full. The remaining MVs are cached at μ BSs and mBSs until the edge computing resources or caching capacities are fully utilized.

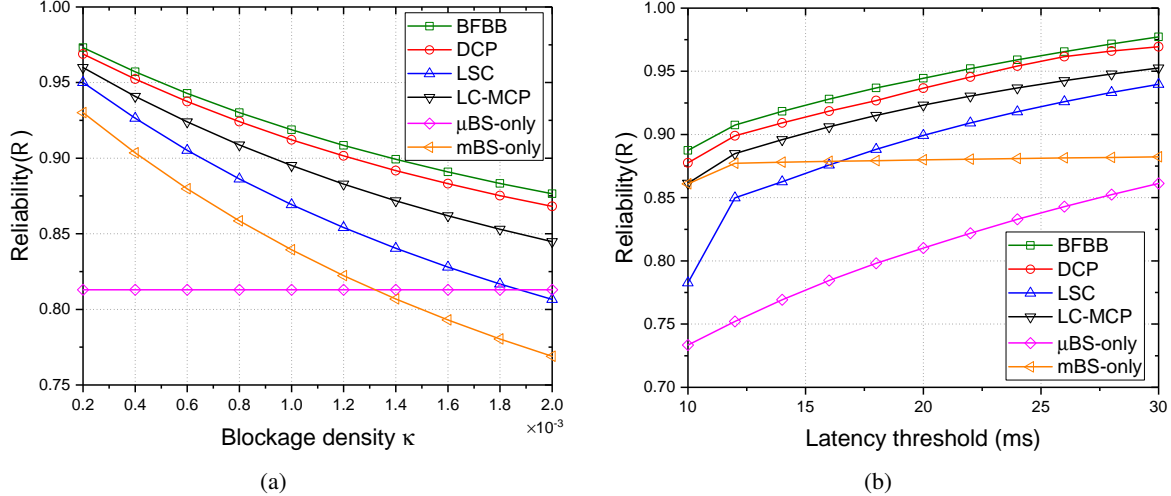


Fig. 2. (a) Reliability of VR delivery versus blockage density κ , and (b) reliability of VR delivery versus latency threshold.

- μ BS-only: Only μ BSs are deployed in the VR delivery network, i.e., let $\lambda_m = 0$, and use the proposed BFBB algorithm to make the joint caching and computing decision.
- mBS-only: Only mBSs are deployed in the VR delivery network, i.e., let $\lambda_\mu = 0$, and use the proposed BFBB algorithm to make the joint caching and computing decision.

A. Reliability Performance

We first evaluate the reliability of VR delivery with various blockage densities as shown in Fig. 2(a). It can be seen that the BFBB algorithm achieves the highest reliability, and the DCP algorithm achieves reliability close to that of the BFBB algorithm. This is because the proposed algorithms comprehensively consider the characteristics of the μ Wave link and the mmWave link to determine a joint caching and computing strategy. It is observed that the performance of LC-MCP is better than that of LSC. This is because caching MVs in the HMD can save more caching capacity and more viewpoints can be cached. Using the local computing capability of the HMD can help more viewpoints to be played in time. The mBS-only can achieve performance close to the proposed algorithms when the blockage density is low, while the performance is significantly reduced when the blockage density is increased. This is because the blockage effect in the mmWave tier causes the link rate to drop rapidly, and the viewpoints cannot be transmitted through the relatively stable μ Wave link, which makes the reliability of VR delivery very low. In contrast, μ BS-only is not affected by the blockage density, so the reliability does not change.

Fig. 2(b) shows the reliability of VR delivery with various delay thresholds. It can be seen that the proposed BFBB and DCP algorithms also achieve higher reliability. The performance of

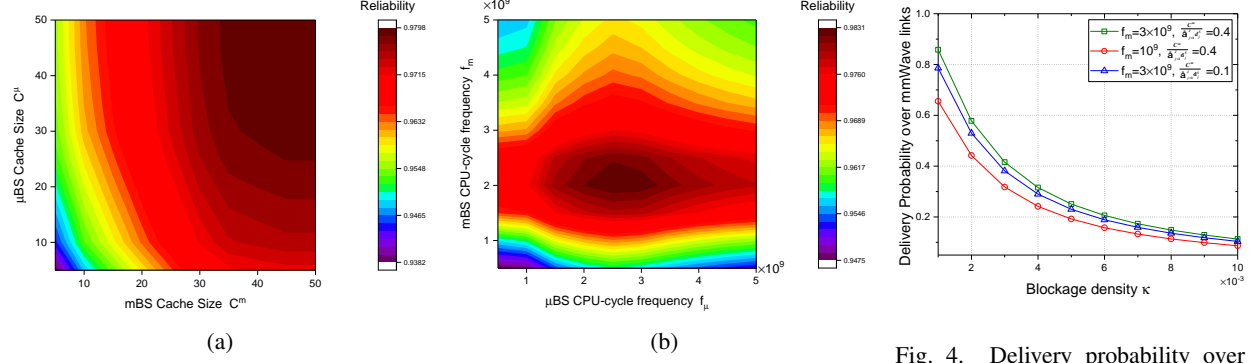


Fig. 3. (a) Reliability of VR delivery for various cache size of μ BSs and mBSs, and (b) reliability of VR delivery for various CPU-cycle frequency of μ BSs and mBSs.

Fig. 4. Delivery probability over mmWave links for various mmWave network parameters.

LC-MCP is better than that of LSC, especially when the delay threshold is low. This is because LC-MCP can cache more viewpoints locally or at BSs, eliminating the backhaul retrieve delay, which is more important when the delay threshold is low. Observing the μ BS-only and mBS-only algorithms, it is seen that mBS-only basically does not change with the increase of the delay threshold, while μ BS-only increases much with the increase of the delay threshold. This indicates that the CDFs of the coverage probabilities of the two channels have different characteristics, and it is necessary to combine the complementary advantages of the two channels to achieve higher reliability.

The impact of caching capacities of μ BSs and mBSs on the reliability of VR delivery is shown in Fig. 3(a). In general, the reliability is higher with a larger caching capacity. It is observed that the caching capacity has a greater gain in the reliability of VR delivery over mmWave links. For example, the reliability is about 0.97 when $C^\mu = 10, C^m = 50$, while the reliability is about 0.95 when $C^\mu = 50, C^m = 10$. This is because the SVs cached at mBSs can be delivered over large-bandwidth mmWave links, so that the SVs can be delivered to the HMD in time.

Fig. 3(b) shows the impact of CPU-cycle frequency of μ BSs and mBSs on the reliability of VR delivery. It is observed that, it is not that the higher the CPU-cycle frequency, the higher the reliability can be obtained. The reason is analyzed in conjunction with the energy consumption limitation in the following subsection. Note that the reliability of VR delivery is more sensitive to f_m compared with f_μ . In other words, the impact on the reliability is greater when f_m is changed. This is because the mBSs needs to consume more computing resources to project and render the MVs into SVs, and deliver them over the large-bandwidth mmWave links. In contrast, the number of MVs computed into SVs at μ BSs is relatively small, which results in less impact on the reliability.

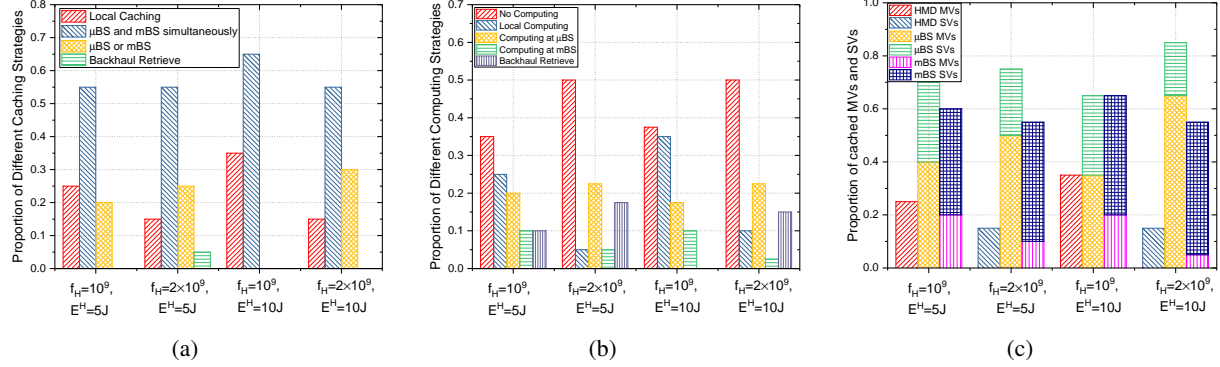


Fig. 5. (a) Proportion of different caching strategies under various f_H and E^H , (b) proportion of different computing strategies under various f_H and E^H , and (c) proportion of cached MVs and SVs under various f_H and E^H .

B. Delivery Probability

The delivery probability over mmWave links is validated with various network parameters as shown in Fig. 4. It can be observed that the delivery probability over mBSs decreases with the increase of the blockage density due to the deteriorating channel conditions, which reflects the importance of μ Wave links to enhance the reliability of VR delivery despite the large mmWave bandwidth. In addition, the delivery probability over mBSs increases when the CPU-cycle frequency or the caching capacity of mBSs increases. This is because the increase in caching and computing resources reduces the average end-to-end delay, thus more viewpoints are delivered over mmWave links according to the minimum delay criterion.

C. Caching and Computing Strategies

We now evaluate the caching and computing strategies to obtain design insights. Fig. 5(a) shows the proportion of different caching strategies under various f_H and E^H . It can be seen that the locally cached viewpoints decrease when the local CPU-cycle frequency f_H increases. This is due to the local energy consumption limitation. Higher computing frequency leads to higher energy consumption, as shown in Fig. 5(b). Therefore, the proportion of local computing should be reduced, otherwise it will cause HMD to heat up and reduce the user experience. Thus, more SVs are cached in the HMD. On the other hand, when f_H is unchanged and E^H is increased, the proportion of local caching or simultaneously cached in μ BS and mBS increases. This is because the local energy consumption limitation is loosen, and more MVs can be cached locally or at BSs. Then more MVs are delivered to the HMD over μ Wave link or mmWave links and computed into SVs locally, as shown in the proportion of local computing in Fig. 5(b). It is worth noting that when $f_H = 10^9$, the proportion of cached at μ BS or mBS decreases with the

increase of E^H . This is because the energy consumption limitation is strict at HMD when E^H is small, thus more SVs should be cached in the limited caching capacity at μ BSs and mBSs to avoid the backhaul retrieve delay. When E^H increases, more MVs can be cached, so more viewpoints can be cached simultaneously at μ BSs and mBSs.

The proportion of cached MVs and SVs under various f_H and E^H is shown in Fig. 5(c). It can be seen that SVs are mainly cached at mBSs, while MVs are more cached at μ BS. This indicates that it is beneficial to cache more SVs at mBSs and deliver them over mmWave links, while cache more MVs at μ BSs and deliver them over μ Wave links. This is reasonable, because delivering more SVs over mmWave links will not increase the transmission delay much due to the large mmWave bandwidth, and the computing delay is saved. On the contrary, more MVs can be delivered over μ Wave links due to the relatively low bandwidth.

VI. CONCLUSION

In this paper, we propose a dual-connectivity μ Wave-mmWave HetNet architecture empowered by mobile edge capability, with the aim of improving the reliability of VR delivery. Based on the differentiated characteristics of μ Wave links and mmWave links, we utilize their complementary advantages to conduct a collaborative design to improve the reliability of VR delivery. From the perspective of stochastic geometry, we first derive closed-form expressions for the reliability of VR delivery. We propose a link selection strategy based on the minimum-delay delivery, and derive the VR delivery probability over μ Wave links and mmWave links. We theoretically show the necessity of μ Wave links to improve the reliability despite the large mmWave bandwidth. We then formulate a joint caching and computing optimization problem to maximize the reliability of VR delivery. By analyzing the coupling caching and computing strategies, we further transform the problem into a MMKP and propose a BFBB algorithm to obtain the optimal solution. To further reduce the complexity of the algorithm, we leverage DCP algorithm to obtain a sub-optimal solution. Numerical results demonstrate the performance improvement using the proposed algorithms, and shows great promise to improve the VR delivery reliability in mobile-edge empowered DC μ Wave-mmWave HetNets.

In future work, a prospective direction is to improve the quality of experience (QoE) for VR users in DC μ Wave-mmWave HetNets. The QoE of VR video transmission is influenced by many factors such as the video rendering, quality of viewpoints, end-to-end delay, and delivery reliability, which is more challenging for modeling and optimization. A QoE-driven cross-layer design framework for mobile-edge empowered DC μ Wave-mmWave HetNets is anticipated, in which resource coordination that dynamically adapts to network conditions can be designed to achieve QoE enhancement.

APPENDIX A

PROOF OF PROPOSITION 1

According to (1) and (11), the reliability of VR delivery over μ Wave links can be derived as

$$\begin{aligned}\mathcal{R}_j^\mu(D_j^\mu, T_j^{\mu,t}) &= \mathbb{P}\left[\frac{P_\mu h_j^\mu r^{-\alpha_\mu}}{I_j^\mu + \sigma_\mu^2} > \nu_j^\mu\right] = \int_0^\infty \mathbb{P}\left[\frac{P_\mu h_j^\mu r^{-\alpha_\mu}}{I_j^\mu + \sigma_\mu^2} > \nu_j^\mu \mid r\right] f_r(r) dr, \\ &\stackrel{(a)}{=} \int_0^\infty e^{-\pi\lambda_\mu r^2} e^{-\nu_j^\mu r^{\alpha_\mu} P_\mu^{-1} \sigma_\mu^2} \mathcal{L}_{I_r}(\nu_j^\mu r^{\alpha_\mu} P_\mu^{-1}) \cdot 2\pi\lambda_\mu r dr, \end{aligned}\quad (34)$$

where (a) follows by using the fact that h_j^μ obeys exponential distribution, and $\mathcal{L}_{I_r}(\nu_j^\mu r^{\alpha_\mu} P_\mu^{-1})$ is the Laplace transform of random variable I_r . Let $s = \nu_j^\mu r^{\alpha_\mu} P_\mu^{-1}$, we have

$$\begin{aligned}\mathcal{L}_{I_r}(\nu_j^\mu r^{\alpha_\mu} P_\mu^{-1}) &= \mathbb{E}_{\Phi_\mu, h}[e^{-sI_r}] = \mathbb{E}_{\Phi_\mu} \left[\prod_{x \in \Phi_\mu \setminus b(o, r)} \frac{s\ell(x)}{1 + s\ell(x)} \right] \stackrel{(b)}{=} \exp\left(-2\pi\lambda_\mu \int_r^\infty \frac{sx}{s + x^{\alpha_\mu}} dx\right), \\ &\stackrel{(c)}{=} \exp(\pi\lambda_\mu s^{\delta_\mu} \Gamma(1 + \delta_\mu) \Gamma(1 - \delta_\mu) - \pi\lambda_\mu r^2 H_{\delta_\mu}(r^{\alpha_\mu} / s)),\end{aligned}$$

where $\ell(x) = x^{-\alpha_\mu}$, $\delta_\mu = 2/\alpha_\mu$. (b) follows from the probability generating functional (PGFL) of the PPP [34], and (c) follows from the use of gamma function or Gauss hypergeometric function for integration, where $H_\delta(x) \triangleq {}_2F_1(1, \delta; 1 + \delta; -x)$ is the Gauss hypergeometric function. By applying the Gauss-Laguerre Quadrature [35], the desired proof is obtained.

APPENDIX B

PROOF OF PROPOSITION 2

According to (4) and (11), the reliability of VR delivery over mmWave links is derived as

$$\begin{aligned}\mathcal{R}_j^m(D_j^m, T_j^{m,t}) &= \mathbb{P}\left[\frac{P_m h_j^m G r^{-\alpha_m}}{I_j^m + \sigma_m^2} > \nu_j^m\right], \\ &\stackrel{(d)}{=} \int_0^\infty \sum_{i \in \{L, N\}} \rho_i(r) \left\{ 1 - \mathbb{E}_{I_j^m} \left[\left(1 - \exp\left(-\frac{\eta_i \nu_j^m r^{\alpha_i} (I_j^m + \sigma_m^2)}{P_m G}\right) \right)^{N_i} \right] \right\} f_r(r) dr, \\ &\stackrel{(e)}{=} \int_0^\infty \sum_{i \in \{L, N\}} \rho_i(r) \left\{ \sum_{k=1}^{N_i} (-1)^{k+1} \binom{N_i}{k} e^{-\frac{k\eta_i \nu_j^m r^{\alpha_i} \sigma_m^2}{P_m G}} \mathcal{L}_{I_j^m}\left(\frac{k\eta_i \nu_j^m r^{\alpha_i} \sigma_m^2}{P_m G}\right) \right\} f_r(r) dr,\end{aligned}$$

where (d) follows from the Alzer's approximation of a gamma random variable [36]. (e) follows by using Binomial theorem and the assumption that N_i is an integer.

$$\begin{aligned}\mathcal{L}_{I_j^m}(s_i) &\stackrel{(f)}{=} \mathbb{E}_{I_j^m} \left[\prod_{\ell \in \Phi_m \setminus b_m} \mathbb{E}_h \left[\exp\left(-s_i h_\ell P_m G r^{-\alpha_i}\right) \right] \right], \\ &\stackrel{(g)}{=} \exp \left[-2\pi\lambda_m p_G \int_r^\infty \left(1 - \mathbb{E}_h \left[e^{-s_i h_\ell P_m G t^{-\alpha_i}} \right] \right) t dt \right], \\ &\stackrel{(h)}{=} \exp \left[-2\pi\lambda_m p_G \int_r^\infty \left(1 - \frac{1}{(1 + s_i P_m G t^{-\alpha_i} / N_i)^{N_i}} \right) t dt \right],\end{aligned}\quad (35)$$

where (f) follows from the i.i.d. distribution of h and the independence of the PPP. (g) follows

by computing the PGFL of the PPP. (h) follows by computing the moment generating function of the gamma random variable h . Applying the integral formula of powers of t and powers of binomials [37], (35) can be written in the form of Gauss hypergeometric function, then the desired result is obtained.

REFERENCES

- [1] F. Hu, Y. Deng, W. Saad, M. Bennis, and A. H. Aghvami, “Cellular-connected wireless virtual reality: Requirements, challenges, and solutions,” *IEEE Communications Magazine*, vol. 58, no. 5, pp. 105–111, 2020.
- [2] M. S. Elbamby, C. Perfecto, M. Bennis, and K. Doppler, “Toward low-latency and ultra-reliable virtual reality,” *IEEE Network*, vol. 32, no. 2, pp. 78–84, 2018.
- [3] A. TaghaviNasrabadi, A. Mahzari, J. D. Beshay, and R. Prakash, “Adaptive 360-degree video streaming using layered video coding,” in *2017 IEEE Virtual Reality (VR)*. IEEE, 2017, pp. 347–348.
- [4] B. Han, “Mobile immersive computing: Research challenges and the road ahead,” *IEEE Communications Magazine*, vol. 57, no. 10, pp. 112–118, 2019.
- [5] M. G. Kibria, K. Nguyen, G. P. Villardi, W.-S. Liao, K. Ishizu, and F. Kojima, “A stochastic geometry analysis of multiconnectivity in heterogeneous wireless networks,” *IEEE Transactions on Vehicular Technology*, vol. 67, no. 10, pp. 9734–9746, 2018.
- [6] J. Mei, K. Zheng, L. Zhao, Y. Teng, and X. Wang, “A latency and reliability guaranteed resource allocation scheme for lte v2v communication systems,” *IEEE Transactions on Wireless Communications*, vol. 17, no. 6, pp. 3850–3860, 2018.
- [7] C. Guo, L. Liang, and G. Y. Li, “Resource allocation for vehicular communications with low latency and high reliability,” *IEEE Transactions on Wireless Communications*, vol. 18, no. 8, pp. 3887–3902, 2019.
- [8] P. Popovski, Č. Stefanović, J. J. Nielsen, E. De Carvalho, M. Angelichinoski, K. F. Trillingsgaard, and A.-S. Bana, “Wireless access in ultra-reliable low-latency communication (urllc),” *IEEE Transactions on Communications*, vol. 67, no. 8, pp. 5783–5801, 2019.
- [9] H. Elshaer, M. N. Kulkarni, F. Boccardi, J. G. Andrews, and M. Dohler, “Downlink and uplink cell association with traditional macrocells and millimeter wave small cells,” *IEEE Transactions on Wireless Communications*, vol. 15, no. 9, pp. 6244–6258, 2016.
- [10] O. Semiari, W. Saad, and M. Bennis, “Joint millimeter wave and microwave resources allocation in cellular networks with dual-mode base stations,” *IEEE Transactions on Wireless Communications*, vol. 16, no. 7, pp. 4802–4816, 2017.
- [11] Y. Shi, H. Qu, J. Zhao, and G. Ren, “Downlink dual connectivity approach in mmwave-aided hetnets with minimum rate requirements,” *IEEE Communications Letters*, vol. 22, no. 7, pp. 1470–1473, 2018.
- [12] C. She, Z. Chen, C. Yang, T. Q. Quek, Y. Li, and B. Vucetic, “Improving network availability of ultra-reliable and low-latency communications with multi-connectivity,” *IEEE Transactions on Communications*, vol. 66, no. 11, pp. 5482–5496, 2018.
- [13] A. Wolf, P. Schulz, M. Dörpinghaus, J. C. S. Santos Filho, and G. Fettweis, “How reliable and capable is multi-connectivity?” *IEEE Transactions on Communications*, vol. 67, no. 2, pp. 1506–1520, 2018.
- [14] E. Bastug, M. Bennis, M. Médard, and M. Debbah, “Toward interconnected virtual reality: Opportunities, challenges, and enablers,” *IEEE Communications Magazine*, vol. 55, no. 6, pp. 110–117, 2017.
- [15] S. Mangiante, G. Klas, A. Navon, Z. GuanHua, J. Ran, and M. D. Silva, “Vr is on the edge: How to deliver 360 videos in mobile networks,” in *Proceedings of the Workshop on Virtual Reality and Augmented Reality Network*, 2017, pp. 30–35.
- [16] C. You, K. Huang, H. Chae, and B.-H. Kim, “Energy-efficient resource allocation for mobile-edge computation offloading,” *IEEE Transactions on Wireless Communications*, vol. 16, no. 3, pp. 1397–1411, 2016.

- [17] T. Q. Dinh, J. Tang, Q. D. La, and T. Q. Quek, "Offloading in mobile edge computing: Task allocation and computational frequency scaling," *IEEE Transactions on Communications*, vol. 65, no. 8, pp. 3571–3584, 2017.
- [18] Y. Mao, J. Zhang, S. Song, and K. B. Letaief, "Stochastic joint radio and computational resource management for multi-user mobile-edge computing systems," *IEEE Transactions on Wireless Communications*, vol. 16, no. 9, pp. 5994–6009, 2017.
- [19] C. Wang, C. Liang, F. R. Yu, Q. Chen, and L. Tang, "Computation offloading and resource allocation in wireless cellular networks with mobile edge computing," *IEEE Transactions on Wireless Communications*, vol. 16, no. 8, pp. 4924–4938, 2017.
- [20] S. Bi, L. Huang, and Y.-J. A. Zhang, "Joint optimization of service caching placement and computation offloading in mobile edge computing systems," *IEEE Transactions on Wireless Communications*, 2020.
- [21] Y. Sun, Z. Chen, M. Tao, and H. Liu, "Communications, caching, and computing for mobile virtual reality: Modeling and tradeoff," *IEEE Transactions on Communications*, vol. 67, no. 11, pp. 7573–7586, 2019.
- [22] T. Dang and M. Peng, "Joint radio communication, caching, and computing design for mobile virtual reality delivery in fog radio access networks," *IEEE Journal on Selected Areas in Communications*, vol. 37, no. 7, pp. 1594–1607, 2019.
- [23] J. Chakareski, "Viewport-adaptive scalable multi-user virtual reality mobile-edge streaming," *IEEE Transactions on Image Processing*, vol. 29, pp. 6330–6342, 2020.
- [24] O. Semiari, W. Saad, M. Bennis, and M. Debbah, "Integrated millimeter wave and sub-6 ghz wireless networks: A roadmap for joint mobile broadband and ultra-reliable low-latency communications," *IEEE Wireless Communications*, vol. 26, no. 2, pp. 109–115, 2019.
- [25] T. Bai and R. W. Heath, "Coverage and rate analysis for millimeter-wave cellular networks," *IEEE Transactions on Wireless Communications*, vol. 14, no. 2, pp. 1100–1114, 2014.
- [26] T. Bai, R. Vaze, and R. W. Heath, "Analysis of blockage effects on urban cellular networks," *IEEE Transactions on Wireless Communications*, vol. 13, no. 9, pp. 5070–5083, 2014.
- [27] M. Di Renzo, "Stochastic geometry modeling and analysis of multi-tier millimeter wave cellular networks," *IEEE Transactions on Wireless Communications*, vol. 14, no. 9, pp. 5038–5057, Sep. 2015.
- [28] U. Niesen and M. A. Maddah-Ali, "Coded caching with nonuniform demands," *IEEE Transactions on Information Theory*, vol. 63, no. 2, pp. 1146–1158, 2016.
- [29] Z. Gu, H. Lu, and Z. Zhu, "On throughput optimization and bound analysis in cache-enabled fiber-wireless networks," *IEEE Transactions on Vehicular Technology*, vol. 69, no. 8, pp. 9068–9082, 2020.
- [30] 3GPP, "5G; Service requirements for next generation new services and markets," 3rd Generation Partnership Project, Rel 15, Tech. Rep., 2018.
- [31] R. Parra-Hernandez and N. J. Dimopoulos, "A new heuristic for solving the multichoice multidimensional knapsack problem," *IEEE Transactions on Systems, Man, and Cybernetics-Part A: Systems and Humans*, vol. 35, no. 5, pp. 708–717, 2005.
- [32] H. A. Le Thi, T. P. Dinh, and H. Van Ngai, "Exact penalty and error bounds in dc programming," *Journal of Global Optimization*, vol. 52, no. 3, pp. 509–535, 2012.
- [33] S. Boyd and L. Vandenberghe, *Convex optimization*. Cambridge university press, 2004.
- [34] S. N. Chiu, D. Stoyan, W. S. Kendall, and J. Mecke, *Stochastic geometry and its applications*. John Wiley & Sons, 2013.
- [35] G. H. Golub, "Calculation of gauss quadrature rules," *Mathematics of computation*, vol. 23, no. 106, pp. 221–230, 1969.
- [36] H. Alzer, "On some inequalities for the incomplete gamma function," *Mathematics of Computation*, vol. 66, no. 218, pp. 771–778, 1997.
- [37] I. S. Gradshteyn and I. M. Ryzhik, *Table of integrals, series, and products*. Academic press, 2014.